Eur Biophys J (2010) 39:1597–1603
DOI 10.1007/s00249-010-0617-8

ORIGINAL PAPER

Ristocetin-induced self-aggregation of von Willebrand factor

Massimiliano Papi · Giuseppe Maulucci · Marco De Spirito · Mauro Missori · Giuseppe Arcovito · Stefano Lancellotti · Enrico Di Stasio · Raimondo De Cristofaro · Alessandro Arcovito

Received: 27 January 2010 / Revised: 10 May 2010 / Accepted: 15 June 2010 / Published online: 30 June 2010

Abstract Von Willebrand factor (VWF) is a large multimeric adhesive glycoprotein, with complex roles in thrombosis and hemostasis, present in circulating blood and in secretory granules of endothelial cells and platelets. High shear stress triggers conformational changes responsible for both binding to the platelet receptor glycoprotein GpIb and its self-association, thus supporting the formation of platelet plug under flow. Ristocetin also promotes the interaction of VWF with GpIb and is able to induce platelet aggregation, and thus is largely used to mimic this effect in vitro. In this research paper, we followed the time course of VWF self-association in solution induced by ristocetin binding by light scattering and at the same time we collected atomic force microscopy images to clarify the nature of the assembly that is formed. In fact, this process evolves initially through the formation of fibrils that subsequently interact to form supramolecular structures whose dimensions would be capable of trapping platelets even in the absence of any degree of shear stress or interaction with external surfaces. This intrinsic property, that is the ability to self-aggregate, may be involved in some pathological settings that have been revealed in clinical practice.

M. Papi · G. Maulucci · M. De Spirito · M. Missori · G. Arcovito
Istituto di Fisica, Università Cattolica S. Cuore, Rome, Italy

E. Di Stasio · A. Arcovito
Istituto di Biochimica e Biochimica Clinica, Università Cattolica S. Cuore, Rome, Italy

S. Lancellotti · R. De Cristofaro (✉)
Istituto di Medicina Interna e Geriatria, Centro Ricerche Fisiopatologia dell'Emostasi, Università Cattolica S. Cuore, Rome, Italy
e-mail: rdecristofaro@rm.unicatt.it

Keywords Protein aggregation · Ristocetin · von Willebrand factor · Primary hemostasis · Atomic force microscopy · Light scattering

Introduction

Von Willebrand factor (VWF) plays a key role in primary hemostasis (Matsushita et al. 2000; Sakariassen et al. 1979). This protein derives from a complex gene (180 kb, 52 exons) and is synthesized as pre-pro-VWF, including a 22-residue signal peptide and a 741-residue propeptide (Sadler 1998). VWF undergoes extensive posttranslational processing, glycosylation, and assembly in the endoplasmic reticulum, Golgi, and post-Golgi. It consists of ~250 kDa monomeric subunits, which form disulfide-linked multimers of 500–20,000 kDa. Each VWF subunit contains 2,050 amino acids made up of conserved modular domains. This complex structural organization is fundamental for its functioning in repairing vascular damage; this event is indeed rapidly followed by firm platelet adhesion and their attachment at the site of endothelial injury is primarily modulated by platelet-subendothelium interaction. By virtue of this process, the platelet receptor GpIb binds to the extracellular matrix components through the intermediation of VWF multimers (Ruggeri and Zimmerman 1981). The evident pro-thrombotic risk associated with this protein is mainly avoided as this process does not occur in static conditions and requires pre-activation of soluble VWF. This process involves a conformational change that exposes the binding site for GpIb in the A1 domain of VWF. This activation mechanism is triggered either by mechanical forces, such as the high shear stress (>5,000 s^{-1}) found in arterial circulation, or by interaction with external surfaces and chemicals/snake venoms (Barg

et al. 2007; Matsui and Hamako 2005; Matsushita et al. 2000; Savage et al. 2002; Singh et al. 2006; Ulrichts et al. 2005). 2B von Willebrand disease (2B-VWD) (Groot et al. 2007; Matsushita et al. 2000) also results in a more stabilized and active form of the protein.

High shear stress causes micro- and macro-conformational changes to occur in VWF, transforming it from a globular state into a stretched conformation (Siedlecki et al. 1996). Interaction of the platelet GpIb receptor with the A1-domain of immobilized VWF (Miura et al. 2000) results in initial adhesion, characterized by a continuous surface translocation of the platelets (Savage et al. 1996). This process ultimately leads to stable platelet adhesion by means of interaction with the platelet collagen receptors GPVI and GPIa/IIa (Nieswandt and Watson 2003), activation of the platelet GPIIb/IIIa receptor complex (Savage et al. 2001), and finally platelet aggregation. Notably, the same shear-induced conformational changes also expose a peptide bond in the A2 domain of the VWF molecule that is cleaved by the metalloprotease ADAMTS-13, which proteolyzes the ultra-large VWF multimers, thus limiting their high pro-hemostatic properties (Tsai 2003). Although self-association and aggregation of VWF under high shear stress are already a recognized phenomenon (Singh et al. 2006), the molecular mechanism driving the process has only recently been clarified (Barg et al. 2007; De Luca et al. 2000). VWF multimers undergo a dramatic shape change as a function of the shear rate that is responsible for the formation of VWF fibers, which are organized in spider web-like structures (Schneider et al. 2007). The latter represents an ideal anchor that serves to capture flowing platelets as the primary hemostasis process takes place.

These past studies showed that in all cases the aggregation and web-formation processes are essentially linked to the mechanical force generated by shear. On the other hand, ristocetin or other molecules, such as the venom botrocetin, also promote the interaction of VWF with GPIb. The antibiotic ristocetin is a polyphenol molecule that interacts with the A1 domain of VWF, thus providing a model for changes in VWF conformation that may occur in vivo, as we demonstrated in a recently published paper (Di Stasio et al. 2009). It could also be considered of special interest as a model for the conformational changes that occur in natural VWF molecules affected by the mutations that cause the different forms of type 2B VWD. It is noteworthy that the transition from a globular conformational state of VWF protein to a stretched active one is a very fast process. It occurs in seconds, as induced by both mechanical (shear stress) and chemical (ristocetin or botrocetin) effectors. In this paper, using atomic force microscopy (AFM) and light scattering (LS), we investigated the slower morphological changes of VWF multimers occurring in the presence of ristocetin to assess the ability of VWF to self-assemble in solution as a function of allosteric modulators and possibly of type 2B mutations, even in the absence of hydrodynamic shear stress.

Materials and methods

VWF purification and characterization

VWF was purified from fresh frozen plasma of type A- or B-specific blood of healthy volunteers by glycine salt precipitation and gel filtration, following the procedure described elsewhere (Tsai 1996). Electrophoresis of VWF in agarose gels containing sodium dodecyl sulfate (SDS-agarose) was performed as previously described (Ruggeri and Zimmerman 1981) with minor changes (Di Stasio et al. 2009) to verify the polydispersity of the sample.

Final protein concentration was determined by UV absorbance at 280 nm on a double beam Varian model Cary 2200 spectrophotometer (Palo Alto, CA), using extinction coefficients (ε) calculated on the basis of the amino acid composition of the VWF monomer. The calculated ε value for VWF was equal to ε (0.1%) = 0.846. The sample was diluted with 10 mM Hepes buffer pH 7.0 (containing 5 mM $CaCl_2$ and 125 mM NaCl) to a final concentration of 0.5 μM. This VWF solution was used to record the time zero in the kinetics experiments. A ristocetin standard solution was added to the sample (final concentration 3 mg/ml) in order to induce maximum conformational change in VWF. After ristocetin was added, the final concentration of VWF was 0.4 μM.

Ristocetin (Helena Laboratories, Beaumont, TX) standard solution (16 mg/ml) was prepared and freed of sulphate ions, as previously detailed (De Cristofaro et al. 2005). The molarity of the ristocetin solution was calculated using a molecular mass value of 2,166 Da and an ε value (0.1%, w/v) at 280 nm equal to 4.41.

Static light scattering

Static light-scattering measurements were performed during VWF aggregation by using a computer-interfaced scattering system ALV-125 (ALV, Langen, Germany). In light scattering experiments, the light scattered out of the incident beam is due to the presence of local fluctuations of dielectric constant over the entire scattering volume and, in the case of diluted solutions, these fluctuations depend on the size and shape of the scattering particles. Static light scattering (Kerker 1969) therefore measures the time-averaged scattered intensity, I, as a function of the scattering wave vector $q = (4\pi n/\lambda)\sin(\vartheta/2)$ where θ is the scattering angle, λ is the laser wavelength, and n the refractive index.

The scattered intensity can be expressed as the convolution of the single particle correlation function and the pair correlation function (Kerker 1969):

$$I(q) \approx P(q)S(q) \quad (1)$$

where $P(q)$ is the form factor and $S(q)$ the structure factor.

Let us now image micro-gels as a collection of fibers made of an assembly of "building blocks" that can be sketched as cylindrical objects with diameter d and length l (Fig. 1). A fiber is made of many segments joined together end-to-end within two branching points. Thus we expect that the average fiber length is much longer than the segment length l, the latter being likely related to the persistence length of the fibers (Ferri et al. 2001, 2002).

When our techniques access the fractal regime $qd \ll 1$, the behavior of $I(q)$ is determined only by the spatial correlations of the segments (Papi et al. 2005), thus:

$$I(q) = Aq^{-d_f} \quad (2)$$

where

$$A = Kc_F\mu l^{(1-d_f)}\pi^{d_f} \quad (3)$$

Here K is the optical constant given by $K = (4\pi^2/\lambda^4 N_A)\, n^2(\partial n/\partial c)^2$ with N_A being Avogadro's number, c_F the sample concentration, and $(\partial n/\partial c)$ the refractive index increment of the solute.

The mass per unit length ratio of the segments, μ, is defined as $\mu = N_A\pi\rho d^2/4$. The diameter d and the density ρ of the segments represent the corresponding parameters of the fibers. It could be noteworthy to observe that since within a single aggregation l is nearly a constant (Ferri et al. 2001, 2002), and the normalized amplitude (A/A_0) is proportional to μ. Furthermore in the case of homogeneous fibril packaging, A/A_0 is even directly proportional to the fibril diameter.

Quasi-elastic light scattering

Quasi light scattering technique measures the intensity autocorrelation function $g_2(\tau) = \langle I(t)I(t+\tau)\rangle/\langle I\rangle^2$ where τ is the lag time and brackets represent the ensemble average. The $g_2(\tau)$ function can be related to the field autocorrelation function $g_1(\tau)$ through the Siegert relation $g_2(\tau) = 1 + \beta g_1^2(\tau)$ where β is an instrumental constant (in our set-up, $\beta = 1$). The mathematical form of $g_1(\tau)$ depends on the physical properties of the investigated system. For monodisperse particles, the density autocorrelation function decays exponentially following $g_1(\tau) = e^{-\Gamma\tau}$, where the decay rate Γ depends on the particle translational diffusion coefficient according to $\Gamma = Dq^2$. For a polydisperse sample, $g_1(\tau)$ is more complex than a single exponential. In this case the distribution of decay rates must be accounted for by introducing a weighting function (A):

$$g_1(\tau) = \int_0^\infty p_I(r_h)e^{-\Gamma(r_h)\tau}dr_h \quad (4)$$

where $p_I(r_h)$ is the normalized intensity-weighted radius distribution function describing the distribution of the fraction of the intensity scattered by a particle of hydrodynamic radius r_h and decay rate $\Gamma(r_h)$, given by:

$$\Gamma(r_h) = kTq^2/6\pi\eta r_h \quad (5)$$

where η is the water viscosity and k the Boltzman constant.

The recovery of the $p_I(r_h)$ distribution, a classical hill-posed problem, can be obtained by the regularized Laplace inversion of the intensity autocorrelation function (Maulucci et al. 2005). In this case, the intensity-weighted radius distribution is obtained by a direct numerical inversion of the DLS data.

Atomic force microscopy

Atomic force imaging was performed by an SPMagic SX atomic force microscope (Elbatech, Italy) in the contact operation mode. The samples were maintained on a glass coverslip in an aqueous environment by just gently adding a drop of buffer on the sample's surface; the measurements were taken at $T = 310$ K . We did not wash the sample after the deposition to avoid the shear stress induced by the buffer flow that could modify the structure of the macro-aggregates. The microscope probe consisted of an ultra-sharp silicon nitride cantilever of a calibrated force constant $k = 0.05$ N/m with a tip radius of less than 10 nm (MikroMash). Image analysis was performed with WSxM software (Nanotec Electronica, Spain).

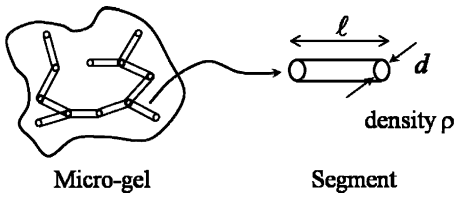

Fig. 1 Sketch of the micro-gel structure. The micro-gel is a fractal assembly of segments of length l, diameter d, and density ρ, joined together end-to-end with only a few branching points. The segment length should not be confused with the average fiber length between the branching points but is rather likely related to the persistence length of the fiber

Results and discussion

Light scattering is established as a technique for the investigation of protein aggregation in solution (De Spirito et al. 2003, 2006; Parasassi et al. 2008). The scattered

intensity from VWF solutions was collected at several angles corresponding to wave vectors q in the range $0.46 \times 10^5 < q < 2.5 \times 10^5$ cm^{-1} and is reported in the inset of Fig. 2 as a function of q. Measurements were performed at different times after the addition of ristocetin in order to study VWF's chemically induced self-aggregation process. Just after the addition of ristocetin, within the span of time required to complete the first angular run (about 180 s), there was an increase in the scattered intensity. This is attributed to the conformational change (Shankaran et al. 2003) from a globular to a stretched conformer that is responsible for the exposure of the binding site to other VWF multimers. Very recently, the group of Schneider (2007) thoroughly investigated the reverse process via the relaxation of ultra-large VWF bundles in a microfluidic-AFM hybrid reactor. Notably this retraction process is completed on a time scale of about 100 s in good agreement with our data (Steppich et al. 2008). Moreover, intensity distribution shapes are well captured by Eq. 2, where A is a constant proportional to the mass-to-length ratio μ and d_f is the fractal dimension (Ferri et al. 2001, 2002; Papi et al. 2005).

The time evolution of A and d_f (Fig. 2) reveals the thickening of elongated structures formed early on, as indicated by the increase in A by three orders of magnitude,

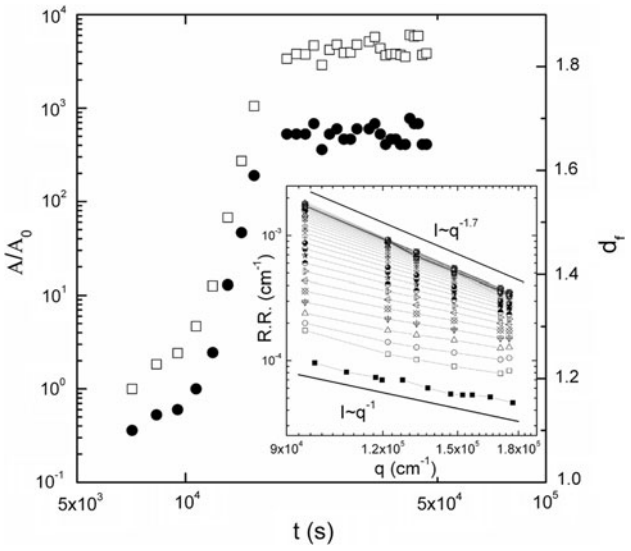

Fig. 2 Span of time covered by VWF aggregation upon ristocetin addition in light-scattering experiments: normalized amplitude A/A_0 (*squares*, *left ordinate*) and fractal dimension d_f (*circles*, *right ordinate*) increase with time, eventually reaching a plateau. *Inset*: Log-log plot of the scattered intensity distributions versus q during the time span covered by aggregation; the *filled squares*, at the *bottom of the inset*, represent data in the absence of ristocetin. Slopes, ranging from -1 to -1.7, represent the mass fractal dimension d_f of the aggregates and clearly show an evolution in the polymers' branching. In the meantime, the amplitude increases, showing a thickening of the VWF, with the growth of elongated structures

with a contextual increase in branching as demonstrated by the fractal dimension variation ranging from 1 to 1.7 (Ferri et al. 2001) (see Fig. 2).

To gain further insight into the growing mechanisms, AFM images were collected both prior to and at different intervals following ristocetin addition. The elongation, branching, and thickening of the structures, resulting from a self-assembly of VWF protein [already characterized by LS in this work and in a previous paper (Di Stasio et al. 2009)], are shown in the images composing Fig. 3 (a–c). Moreover, on larger time scales (d, e), these structures further evolve to become more and more compact, thereby creating local micro-gel structures that finally overlap. By combining AFM and LS measurements, we can therefore show that the aggregation mechanism consists of an initial fibril formation, at short length scales and terminating after about 2 h, which then evolves by forming a micro-gel throughout the aggregation process. The aggregation's driving mechanism, i.e., fibril formation (Brunelli et al. 2007), can be further investigated by means of a quantitative analysis of AFM images (see Fig. 4). In the absence of ristocetin (Fig. 4a, b), VWF assumes its resting state and is characterized by the presence of a large polydispersed family of protein with an average radius of $R_{AFM} = 25 \pm 7$ nm. In the same panel, quasi elastic light scattering confirms, albeit through increased statistics, the observed size distribution with an average radius of $R_{LS} = 19 \pm 5$ nm. These results correspond well to the pattern of VWF multimers observed in gel electrophoresis and confirm previous findings obtained using electron microscopy, small angle neutron scattering, turbidimetry, and light scattering (Di Stasio et al. 2009; Loscalzo et al. 1985; Singh et al. 2006; Slayter et al. 1985).

Later on, 1 h after the addition of ristocetin (Fig. 4c, d), elongated and branched fibrils are clearly observable. Fibril radius has a size distribution that ranges from the value corresponding to that of the smaller VWF molecules to about twice that of the larger ones, with an average of $R_{fib} = 34 \pm 15$ nm. Thus, early fibrils occur by means of an ordered binding of VWF molecules in a pearl necklace manner. Control experiments performed under the same experimental conditions but in the absence of ristocetin showed that no conformational changes occurred in VWF molecules (data not shown).

The transformation of multimeric plasma-derived VWF into a widespread immobile network is dependent on several physical and biochemical factors; these factors are chiefly represented in vivo by matrix proteins (Barg et al. 2007). Under shear, after a rodlike/random coil transition (Shankaran et al. 2003), VWF can form a spider web-like network, which represents an optimal structure onto which circulating platelets can anchor and thus support primary hemostasis (Raghavachari et al. 2000; Schneider et al. 2007). Moreover,

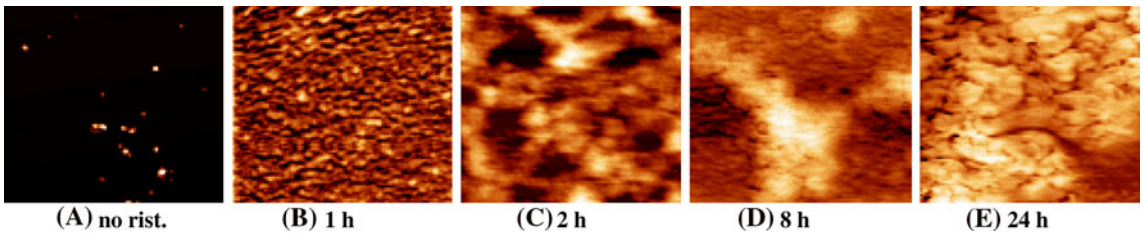

Fig. 3 3.5 × 3.5 μm AFM images of the supramolecular aggregates of VWF protein **a** in the absence of ristocetin and **b** 1, **c** 2, **d** 8, and **e** 24 h after its addition. Supramolecular structures evolve with time from small dispersed aggregates to massive branched structures that became more and more compact over time

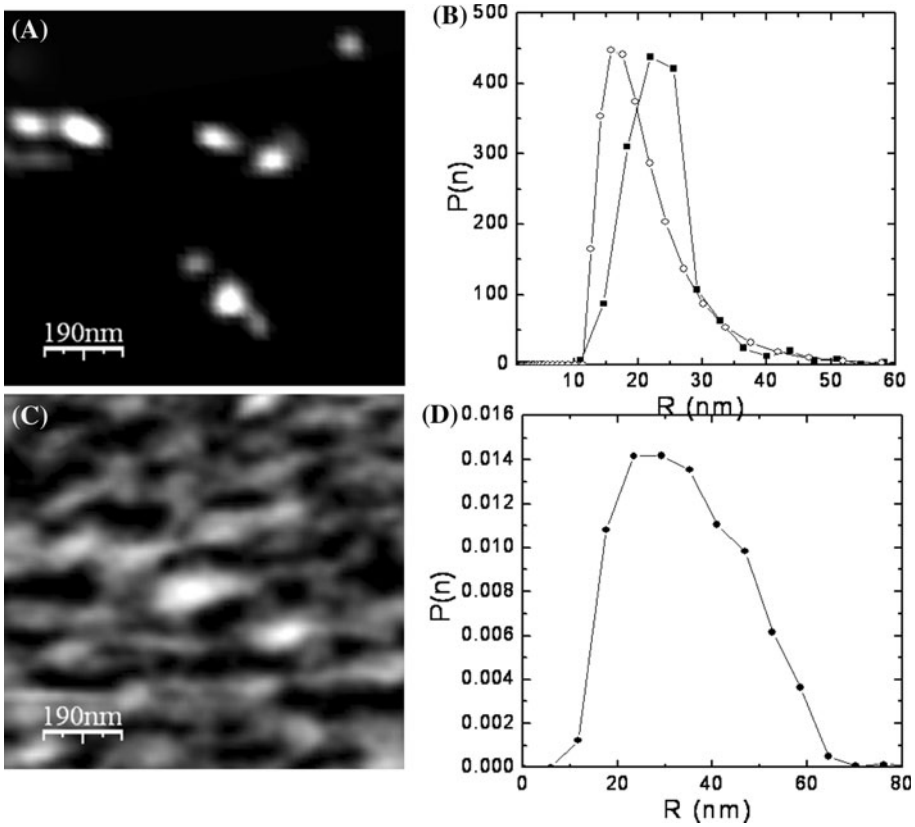

Fig. 4 **a** AFM images of VWF protein in the absence of ristocetin. **b** Size distribution of the VWF in the absence of ristocetin as a result of a statistical analysis of four different AFM images (*closed squares*) and as a result of the dynamic light-scattering size distribution of the hydrodynamic radius (*open circles*). **c** Magnification of AFM image of the supramolecular aggregates of VWF protein after 1 h. **d** Size distribution of the VWF early aggregates as a result of a statistical analysis of four different AFM images. Supramolecular structures evolve with time from small dispersed aggregates to a network characterized by an average fibril radius of 34 nm

VWF solution structure is stabilized by frequent interdomain interactions taking place between *A*-domain residues located on different monomer units (Ulrichts et al. 2005). Such interdomain interactions may be important regulators of VWF's function in physiology and pathology. In this paper we investigated the formation of VWF's spider web-like network: this process seems to evolve initially by forming early fibrils; only later does the branching formation increase, and micro-gel spots, with a characteristic fractal dimension of about 1.7, become evident.

Conclusion

Based on the present findings, we propose that the large conformational changes induced by ristocetin binding disrupt the multiple domain interactions that occur in the globular VWF structure, as demonstrated by our AFM experiments (see Fig. 4a). Upon stabilization of the extended conformation through ristocetin binding, homotypic domain interactions are substituted by heterotypic A-domain associations, which contribute to the formation of the network shown in Fig. 4c. The mechanism is a physical example of the model known as "3D swapping" (Liu and Eisenberg 2002), by means of which the conformational transitions in a multidomain protein alter internal homotypic interactions, thereby allowing heterotypic domain interactions and hence the formation of aggregates. This mechanism optimizes the formation of a spider web-like network, which anchors circulating platelets through binding of the GpIb-IX-V membrane complex. We hypothesize that a different distribution of multimers in

VWF likely affects the efficiency and thus the rate of the network's formation (future experiments will be done to test this statement). Thus, this proposed mechanism may play a relevant role in vivo. In fact, VWF has a mean half-life of about 20 h, a length of time comparable to the period required for the structural rearrangements to manifest.

Moreover, patients with severe aortic stenosis normally present high levels of shear stress across the stenotic valve. These patients usually show low levels of circulating VWF, a phenomenon attributed to an enhanced proteolysis of VWF multimers by the metalloprotease ADAMTS13, which recognizes and cleaves VWF multimers only under shear stress of >30 dyn/cm^2 (Tsai 2003). However, in this setting, the generated high shear stress may also promote aggregation of VWF molecules, thereby contributing to the decrease of circulating VWF levels. Similarly, in particular as regards type 2B VWD, the decreased levels of the ultra-large molecular weight form may arise not only as a consequence of enhanced binding to platelet GpIb, but also as a product of the above mechanism responsible for VWF aggregation. The pathological deposition of these VWF aggregates in micro-circulation may contribute to the thrombo-hemorrhagic syndromes that occur in these clinical settings.

Acknowledgments R.D.C. acknowledges the financial support provided by MIUR (PRIN-2007) and the generous provision of some of the reagents used in this study by Grifols Italia (Ghezzano, Pisa, Italy). M.D.S., G.A., A.A., E.D.S., and R.D.C. were also supported by the funds assigned to the research programs D.1 2006 and 2007 of the Medicine Faculty of Università Cattolica del S. Cuore, Rome, Italy. Experimental data reported in this paper were obtained at the LABCEMI (Laboratorio Centralizzato di Microscopia, Ottica ed Elettronica) of the Università Cattolica del S. Cuore Roma (Italy). (http://webprd.rm.unicatt.it/pls/unicatt_rm/consultazione.mostra_pagina?id_pagina=20215).

References

Barg A, Ossig R, Goerge T, Schneider MF, Schillers H, Oberleithner H, Schneider SW (2007) Soluble plasma-derived von Willebrand factor assembles to a haemostatically active filamentous network. Thromb Haemost 97:514–526

Brunelli R, Papi M, Arcovito G, Bompiani A, Castagnola M, Parasassi T, Sampaolese B, Vincenzoni F, De Spirito M (2007) Globular structure of human ovulatory cervical mucus. FASEB J 21:3872–3876

De Cristofaro R, Peyvandi F, Palla R, Lavoretano S, Lombardi R, Merati G, Romitelli F, Di Stasio E, Mannucci PM (2005) Role of chloride ions in modulation of the interaction between von Willebrand factor and ADAMTS-13. J Biol Chem 280:23295–23302

De Luca M, Facey DA, Favaloro EJ, Hertzberg MS, Whisstock JC, McNally T, Andrews RK, Berndt MC (2000) Structure and function of the von Willebrand factor A1 domain: analysis with monoclonal antibodies reveals distinct binding sites involved in recognition of the platelet membrane glycoprotein Ib-IX-V complex and ristocetin-dependent activation. Blood 95:164–172

De Spirito M, Arcòvito G, Papi M, Rocco M, Ferri F (2003) Small- and wide-angle elastic light scattering study of fibrin structure. J Appl Cryst 36:636–641

De Spirito M, Brunelli M, Mei G, Bertani F, Ciasca G, Greco G, Papi M, Arcovito G, Ursini F, Parasassi T (2006) Low density lipoprotein aged in plasma forms clusters resembling subendothelial droplets: aggregation via surface sites. Biophys J 90:4239–4247

Di Stasio E, Romitelli F, Lancellotti S, Arcovito A, Giardina B, De Cristofaro R (2009) Kinetic study of von Willebrand factor self-aggregation induced by ristocetin. Biophys Chem 144:101–107

Ferri F, Greco M, Arcovito G, Bassi FA, De Spirito M, Paganini E, Rocco M (2001) Growth kinetics and structure of fibrin gels. Phys Rev E Stat Nonlin Soft Matter Phys 63:031401

Ferri F, Greco M, Arcovito G, De Spirito M, Rocco M (2002) Structure of fibrin gels studied by elastic light scattering techniques: dependence of fractal dimension, gel crossover length, fiber diameter, and fiber density on monomer concentration. Phys Rev E Stat Nonlin Soft Matter Phys 66:011913

Groot E, de Groot PG, Fijnheer R, Lenting PJ (2007) The presence of active von Willebrand factor under various pathological conditions. Curr Opin Hematol 14:284–289

Kerker M (1969) The scattering of light and other electromagnetic radiation. Academic, New York

Liu Y, Eisenberg D (2002) 3D domain swapping: as domains continue to swap. Protein Sci 11:1285–1299

Loscalzo J, Fisch M, Handin RI (1985) Solution studies of the quaternary structure and assembly of human von Willebrand factor. Biochemistry 24:4468–4475

Matsui T, Hamako J (2005) Structure and function of snake venom toxins interacting with human von Willebrand factor. Toxicon 45:1075–1087

Matsushita T, Meyer D, Sadler JE (2000) Localization of von Willebrand factor-binding sites for platelet glycoprotein Ib and botrocetin by charged-to-alanine scanning mutagenesis. J Biol Chem 275:11044–11049

Maulucci G, De Spirito M, Arcovito G, Boffi F, Castellano AC, Briganti G (2005) Particle size distribution in DMPC vesicles solutions undergoing different sonication times. Biophys J 88:3545–3550

Miura S, Li CQ, Cao Z, Wang H, Wardell MR, Sadler JE (2000) Interaction of von Willebrand factor domain A1 with platelet glycoprotein Ibalpha-(1–289). Slow intrinsic binding kinetics mediate rapid platelet adhesion. J Biol Chem 275:7539–7546

Nieswandt B, Watson SP (2003) Platelet-collagen interaction: is GPVI the central receptor? Blood 102:449–461

Papi M, Arcovito G, De Spirito M, Amiconi G, Bellelli A, Boumis G (2005) Simultaneous static and dynamic light scattering approach to the characterization of the different fibrin gel structures occurring by changing chloride concentration. Appl Phys Lett 86:183901

Parasassi T, De Spirito M, Mei G, Brunelli R, Greo G, Lenzi L, Maulucci G, Nicolai E, Papi M, Arcovito G, Tosatto SCE, Ursini F (2008) Low density lipoprotein misfolding and amyloidogenesis. FASEB J 22:2350–2356

Raghavachari M, Tsai H, Kottke-Marchant K, Marchant RE (2000) Surface dependent structures of von Willebrand factor observed by AFM under aqueous conditions. Colloids Surf B Biointerfaces 19:315–324

Ruggeri ZM, Zimmerman TS (1981) The complex multimeric composition of factor VIII/von Willebrand factor. Blood 57:1140–1143

Sadler JE (1998) Biochemistry and genetics of von Willebrand factor. Annu Rev Biochem 67:395–424

Sakariassen KS, Bolhuis PA, Sixma JJ (1979) Human blood platelet adhesion to artery subendothelium is mediated by factor VIII-von Willebrand factor bound to the subendothelium. Nature 279:636–638

Savage B, Saldivar E, Ruggeri ZM (1996) Initiation of platelet adhesion by arrest onto fibrinogen or translocation on von Willebrand factor. Cell 84:289–297

Savage B, Cattaneo M, Ruggeri ZM (2001) Mechanisms of platelet aggregation. Curr Opin Hematol 8:270–276

Savage B, Sixma JJ, Ruggeri ZM (2002) Functional self-association of von Willebrand factor during platelet adhesion under flow. Proc Natl Acad Sci USA 99:425–430

Schneider SW, Nuschele S, Wixforth A, Gorzelanny C, Alexander-Katz A, Netz RR, Schneider MF (2007) Shear-induced unfolding triggers adhesion of von Willebrand factor fibers. Proc Natl Acad Sci USA 104:7899–7903

Shankaran H, Alexandridis P, Neelamegham S (2003) Aspects of hydrodynamic shear regulating shear-induced platelet activation and self-association of von Willebrand factor in suspension. Blood 101:2637–2645

Siedlecki CA, Lestini BJ, Kottke-Marchant KK, Eppell SJ, Wilson DL, Marchant RE (1996) Shear-dependent changes in the three-dimensional structure of human von Willebrand factor. Blood 88:2939–2950

Singh I, Shankaran H, Beauharnois ME, Xiao Z, Alexandridis P, Neelamegham S (2006) Solution structure of human von Willebrand factor studied using small angle neutron scattering. J Biol Chem 281:38266–38275

Slayter H, Loscalzo J, Bockenstedt P, Handin RI (1985) Native conformation of human von Willebrand protein. Analysis by electron microscopy and quasi-elastic light scattering. J Biol Chem 260:8559–8563

Steppich DM, Angerer JI, Sritharan K, Schneider SW, Thalhammer S, Wixforth A, Alexander-Katz A, Schneider MF (2008) Relaxation of ultralarge VWF bundles in a microfluidic-AFM hybrid reactor. Biochem Biophys Res Commun 369:507–512

Tsai HM (1996) Physiologic cleavage of von Willebrand factor by a plasma protease is dependent on its conformation and requires calcium ion. Blood 87:4235–4244

Tsai HM (2003) Shear stress and von Willebrand factor in health and disease. Semin Thromb Hemost 29:479–488

Ulrichts H, Vanhoorelbeke K, Girma JP, Lenting PJ, Vauterin S, Deckmyn H (2005) The von Willebrand factor self-association is modulated by a multiple domain interaction. J Thromb Haemost 3:552–561